Mechanism of O_2 Activation for Conversion of Fatty Acids into Terminal Alkenes in a Membrane-bound Metalloenzyme UndB

Simran Nisha[#1,2], Arunima Choudhury[#1,2] and Subhendu Roy[1, 2*]

[#]These authors contributed equally to this work

[1]Biophysical Sciences Group, Saha Institute of Nuclear Physics, Kolkata 700064, India. [2]Homi Bhabha National Institute, Mumbai 400094, India

Email: subhendu.roy@saha.ac.in

KEYWORDS: Biofuel, O_2 Activation, Nonheme diiron enzymes, Mechanism, Dynamic, Iron Cofactors, QM/MM, Free energy simulations

ABSTRACT:

Biosynthesis of 1-alkenes by a membrane-bound bacterial enzyme UndB from naturally abundant free fatty acids offers a promising route toward the next generation of hydrocarbon-based biofuels and industrially valuable chemicals. UndB is the only known fatty acid decarboxylase to produce 1-alkene, offering a sustainable and eco-friendly avenue for 1-alkene bioproduction. Despite the wide implications of UndB in biofuel production, its mechanism of action is unknown. Herein, we present the catalytic pathway of UndB using a suit of dynamical multiscale simulations in combination with Alphafold3 method. Our analysis reveals for the first time the existence of a dynamic iron cofactors in UndB, capable of forming a peroxodiiron(III/III) intermediate to activate molecular O_2 to carry out a difficult C–H bond-breaking chemical reaction. Large-production of hydrogen peroxide (H_2O_2) during UndB catalysis provide strong support for the formation of this peroxo intermediate, that is further validated by calculated activation barrier with the experimental observation. The origin of regiospecificity of the C-β reaction is attributed to the substrate flexibility in the active conformation. The mechanism is fundamentally different from the proposed canonical pathway in these family of enzymes and in excellent agreement with major experimental results. This study thus opens a new window for mechanistic understanding of such integral membrane enzymes in unprecedented details.

Introduction

Massive energy consumption, depleting resources and global climate change have raised serious concerns regarding continued dependence on fossil fuels as the predominant source of energy and have motivated a tremendous search for developing renewable biofuels(1, 2). Recently, an alkene -producing metalloenzyme, UndB,(3) was discovered from bacterial species *Pseudomonas* species and reported to belong to the fatty acid desaturase (FADS)-like superfamily such as Stearoyl-CoA Desaturase 1 (SCD1) and AlkB (4, 5). This membrane-bound enzyme has gained tremendous attention due to its ability to catalyze highly efficient conversion of a large number of fatty acids to terminal alkenes by breaking a strong C–H bond (bond dissociation energy > 95.0 kcal/mol)(6), which is a very challenging chemical reaction (Fig. 1a). These terminal alkenes, particularly those derived from medium-chain C12-fatty acids can be transported as liquid biofuels, making it an extremely important chemical with energy properties similar to petroleum fuels.

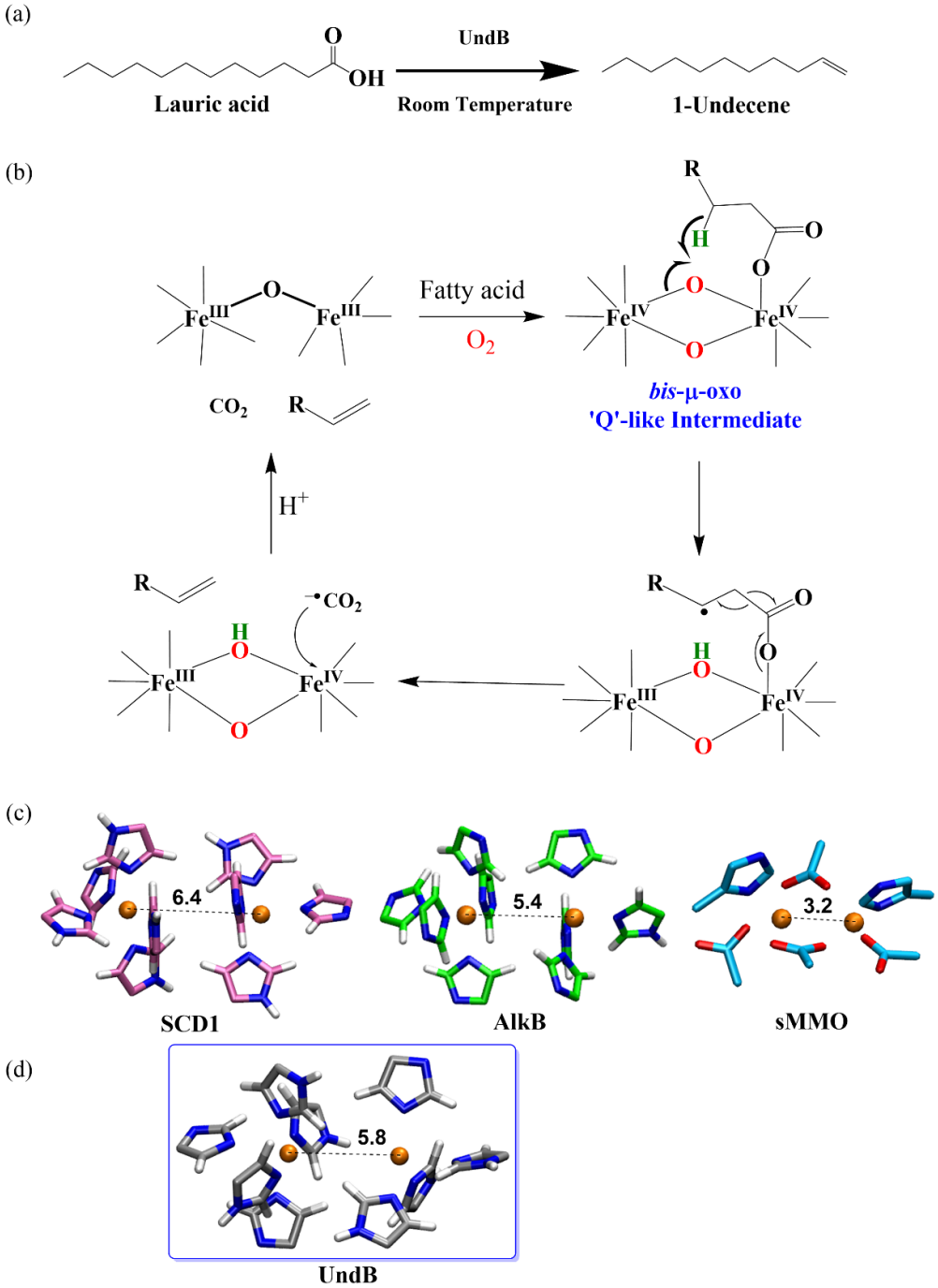

Fig 1. (a) The chemical reaction catalyzed by UndB. (b) Proposed reaction mechanism for conversion of fatty acids into terminal alkenes by UndB. (c) Diiron centres of the active sites of SCD1, AlkB and sMMO with Fe-Fe distances shown in Å. (d) Alphafold3 predicted active site of *Pc*UndB.

Since its discovery in 2015(7), there are no structural and very little mechanistic details reported for UndB (3). The genetic sequence was identified and found to belong to the FADS-superfamily of enzymes containing characteristic nine histidine residues. These nine histidine residues also constitute the active site in SCD1 and AlkB. A generic mechanistic pathway involving the famous 'Q'-like intermediate(8) has been invoked in an attempt to explain the catalytic activity of UndB

based on kinetic studies (Fig 1b).(3) UndB starts the reaction by hydrogen atom abstraction (HAA) from the *β*-carbon of the substrate, and generates a substrate radical. The substrate radical undergoes decarboxylation to generate 1-alkene by one of the following pathways: (i) the cleavage of the radicaloid C1−C2 bond followed by an electron transfer from the generated $CO_2^{\bullet-}$ radical to the diiron (III/IV) to release 1-alkene and CO_2, and regeneration of the active site for the subsequent turnover (3). Two other pathways suggested are a Kolbe-type decarboxylation and a multi-bond fragmentation. However, the authors presented kinetic isotope effects, k_H/k_D=2.6, to establish the HAT process as the rate-determining step (rds) in UndB compared to the Kolbe-type mechanism.

How two Fe (iron) centers become so close for formation of 'Q'-like intermediate with nine conserved histidine active site residues? Is 'Q' being the real oxidant in UndB? There are no answers to these questions, more so after recent discoveries of crystal/Cryo-EM structure and mechanistic revelations of SCD1(9) and AlkB (4, 5, 10). The Fe…Fe distance is 6.4Å-6.8Å in SCD1 that is significantly longer than that in His/Carboxylate active site of ferritin-like diiron oxidase and oxygenase (FDO) family such as soluble methane monooxygenase (sMMO), Δ9-Desaturase and Arylamine N-oxygenases AurF and CmII (Fig. 1c). Similar kinds of histidine rich active site are also found in alkane oxidizing membrane enzyme AlkB with a longer Fe…Fe distance of (5.4-6.1Å)(11). Shorter iron-iron distance is reported to be essential for O_2 activation in most of the non-heme diiron enzymes, making it a crucial structural feature (12, 13).

In SCD1 and AlkB, based on long iron-iron distances as determined by X-ray/Cryo-EM, a canonical mechanism where the two iron ions play different roles has been favoured in contrast to the above 'Q'-like mechanism (Fig. 1b) proposed for UndB. In this, one iron acts as the site of high valent chemistry and the other iron ion serving as a shuttle for protons and electrons for HAA step from the respective substrate (11, 14, 15). This mechanism not only lacks any experimental support but also there are several experimental observations that it cannot explain. The mechanism is particularly confusing (16) from Mössbauer and EPR spectroscopic results in AlkB (10, 17) and SCD1 (18). While AlkB shows a strong presence of anti-ferromagnetic coupling ($J < 80$ cm^{-1}), SCD1 reveals a weak anti-ferromagnetic coupling ($J \sim 7$ cm^{-1}) (14, 19). Herein, there is no clue about whether the same mechanism is operational in UndB as in SCD1 and AlkB. The only certainty in UndB is that the β-hydrogen (β-H) of the substrate must be in reacting distance with the activated O_2 species.

Fueled by this enthralling background, we have embarked on a journey to unravel the mechanistic pathway of UndB using large-scale molecular dynamics (MD), multiscale quantum mechanics/molecular mechanics (QM/MM) free energy simulations and rigorous quantum chemical (QM) calculations in conjunction with Alphafold3 method. This will be the first applications of QM/MM MD simulations to decode the full catalytic pathway and active conformation of a transmembrane $NHFe_2$ enzyme, UndB for which no structural and very little mechanistic data exists. Most importantly, all simulation results are strongly correlated with available experimental data and in quantitative manner wherever feasible. There have been multiple reports pointing towards an unusual O_2 activation mechanism in these kinds of non-heme

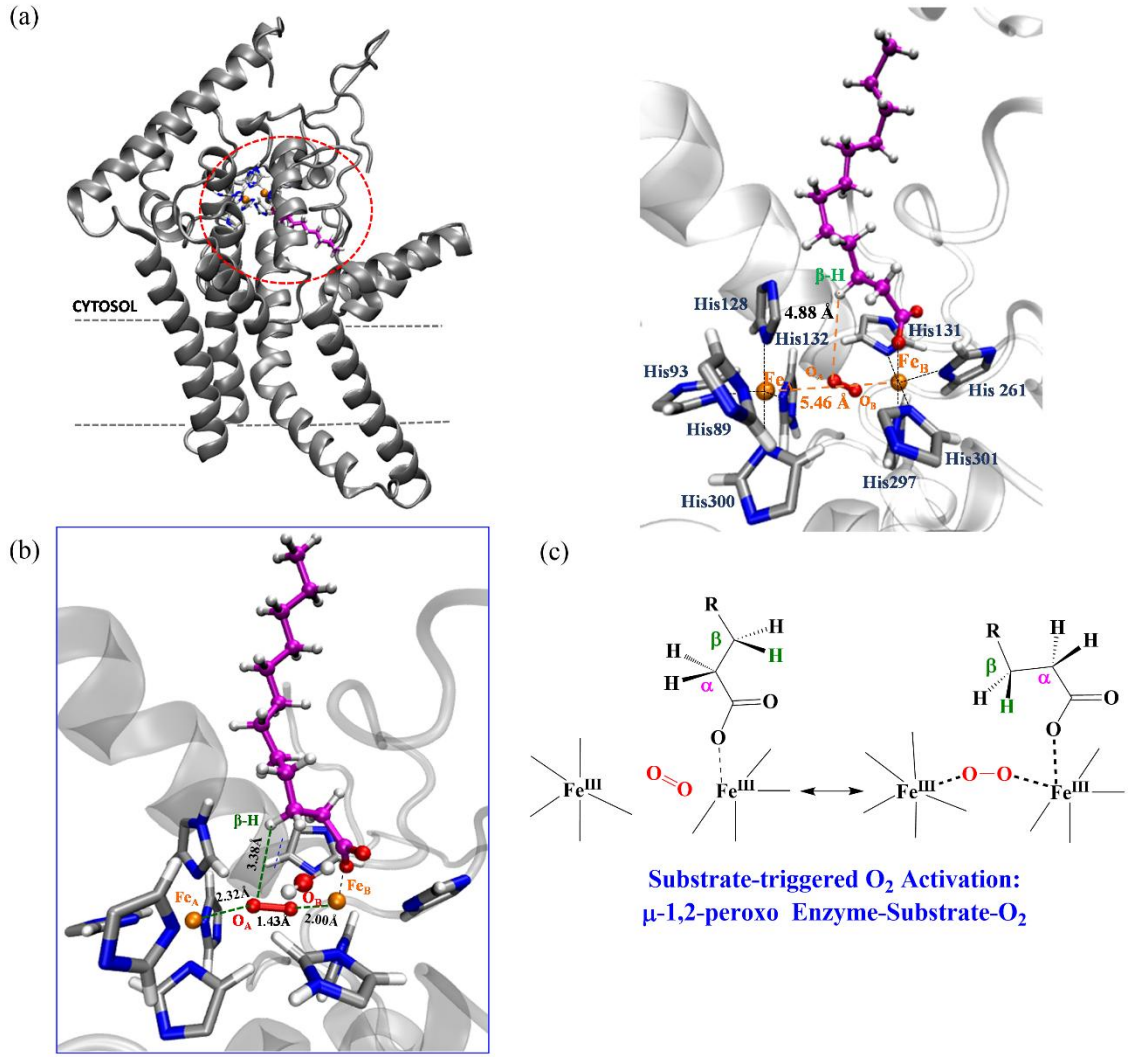

Fig 2. Schematic representation of the (a) UndB embedded in POPC lipid membrane; (Inset) the active site region of the enzyme-substrate-O_2 complex from QM/MM MD simulations in high-spin iron. (b) Peroxodiiron(III/III) intermediate as obtained from the specialized QM/MM MD simulations.

diiron enzymes ($NHFe_2$) enzymes (9, 12), which has so far been intractable to any experimental and computational methods. In this paper, for the first time we have unraveled an unprecedented mechanistic pathway involving dynamic iron cofactors in UndB, that is capable of forming a peroxodiiron(III/III) intermediate by which UndB activates O_2 to produce terminal alkenes. This mechanism, in excellent agreement with experimental data and explain all major experimental findings, is considerably different from the proposed pathway of other $NHFe_2$ enzymes as formation of a *cis*-1,2-peroxo intermediate was presumed unfeasible for SCD1 based on longer Fe…Fe distance and histidine-rich motifs(4) and a recent EXAFS study on AlkB (11, 14). The outcome has crucial implications that goes beyond traditional structure determination of integral membrane enzymes and provide crucial insights into mechanism of this new class of metalloenzymes.

Results and Discussion

Enzyme-Substrate-O_2 (ESO_2) complex of UndB

In the absence of any experimentally determined structural data on UndB, we employed Alphafold3 (AF3) to obtain three-dimensional (3D) structure of UndB incorporating the two iron cofactors(20), using homologous sequences from *Pseudomonas canadensis* (PcUndB) and *Pseudomonas mendocina* (PmUndB) that exhibit 85% sequence similarity. Since both UndB structures have led to similar results, which establishes the robustness of the conclusions of this study, the following results are discussed with respect to PcUndB unless otherwise stated. Alphafold3 has shown ground-breaking successes in accurately predicting 3D structures of membrane enzymes like AlkB(14). Structural integrity of AF3-predcited UndB has been further checked (section 2, SI). The two structures of UndB from two different species revealed an identical Fe…Fe distance of 5.87Å in the substrate-bound form (Fig. 1d). QM/MM free energy simulations of the substrate-unbound UndB gives the most stable Fe…Fe distance to be 5.7Å as discussed later (section 1.5 and methods, SI). The AF3 predicted UndB structure is in good agreement with biochemical characterization that the active site of UndB consists of two non-heme iron metals coordinated entirely by nine histidine residues much like SCD1 and AlkB (3) (Fig. 1c). That study further confirmed it to be a O_2-dependent enzyme along with involvement of suitable electron transport proteins. After cumulative 1.5 microseconds (μs) long classical simulations of multiple UndB replicas, the most probable Fe…Fe distances in UndB comes around 5.10Å and 6.42 Å (Fig S5, SI) in the substrate-O_2-bound UndB. The distance between the iron centers falls in line that of SCD1 (21) and AlkB which was reported to be 6.4-6.8Å and 5.4-6.1Å. These observations indicate that the active site architecture is globally conserved and remains structurally stable, as reflected by the comparable inter-iron distances observed across the family. Moreover, the binding orientation of the substrate, lauric acid, closely matches with the experimentally characterized substrate pose in UndA (6). However, it did not yield a reactive conformation of UndB during the molecular dynamics simulations, as evidenced by the persistently large separation between the bound O_2 molecule and the substrate's β-H atoms (Fig. S4, SI). Consistently, QM/MM molecular dynamics simulations of UndB with lauric acid and O_2 bound to either Fe centres fail to produce any reactive geometry in the most relevant high-spin iron, S = 4 state that was reported for non-heme diiron enzymes (12)(Fig. S5, SI). It holds true even for other spin states (S = 5, 0) considered for multiscale simulations. Throughout the 60 ps simulations, the β-H remains distal from the bound oxygen atoms (Fig. 2a and Fig. S5, SI), whereas molecular O_2 preferentially binds to or transiently hovers over the substrate-bound Fe_B centre, revealing its role as the initial activation site. Notably, a similar non-reactive conformation has been observed in the lauric acid-bound UndA crystal structure, raising the unresolved question of how the reaction is subsequently initiated (6).

The longer Fe…Fe distance has been a structural signature in this new family of $NHFe_2$ enzymes which is contrary to shorter Fe…Fe distances observed in FDO family of enzymes (12, 13), which typically use histidine/carboxylate motifs and primarily carboxylate amino acids as canonical bridging ligands. The longer Fe-Fe distance in a unique histidine-only coordination implies a potentially novel mechanism for activating molecular oxygen (O_2) during the decarboxylation reaction in this family of enzymes (2, 9). It has thus become very enigmatic how O_2 gets activated by canonical two electron reduction process donated by two long-distant iron

cofactors. One also wonders what conformational changes occurs in UndB upon O_2 activation and subsequently perform a chemically challenging C–H bond breaking reaction.

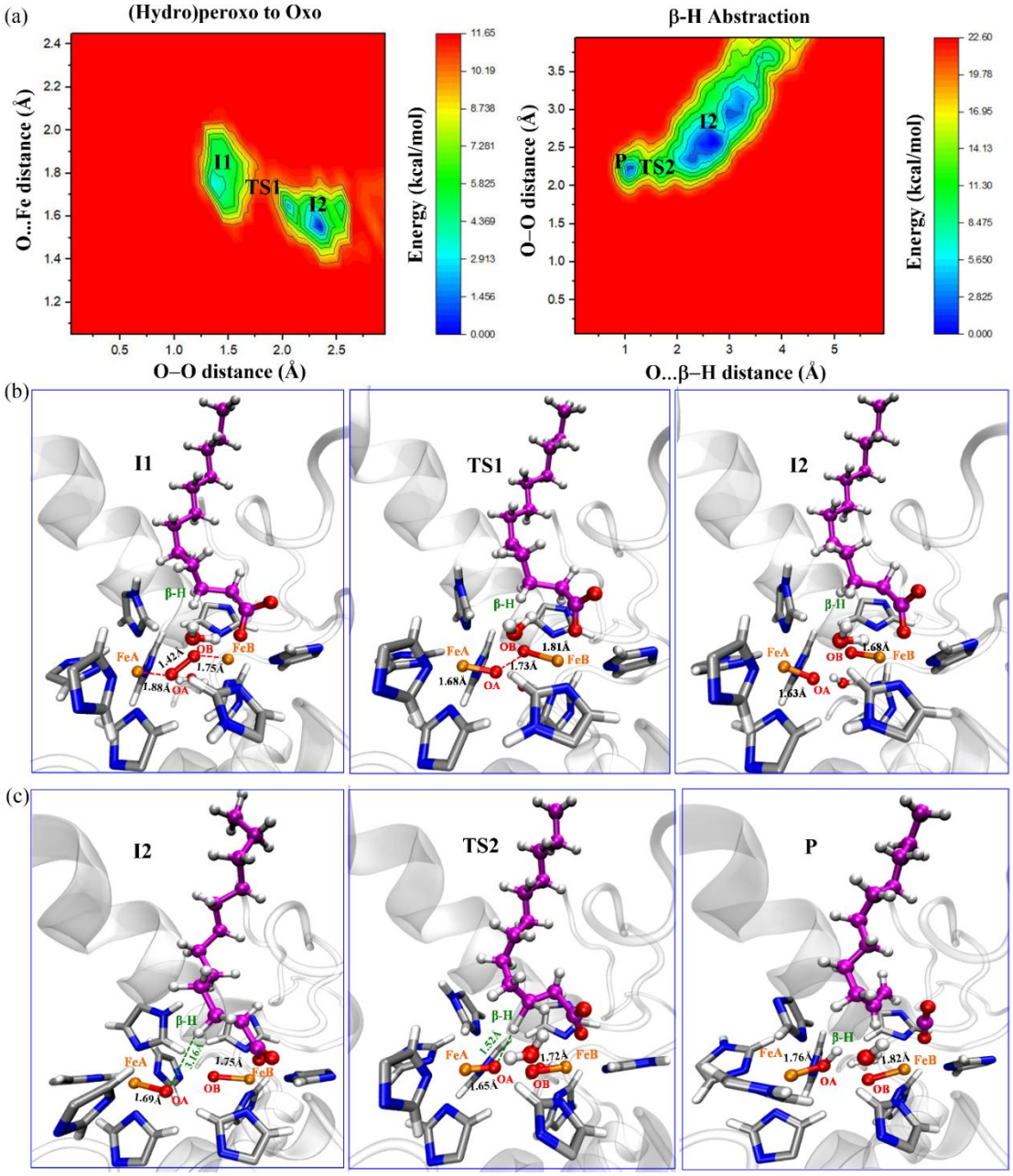

Fig. 3. QM/MM free energy landscape of the rate determining β-H abstraction step in UndB at PM6/CHARMM36 level. (b) Possible intermediates and transition states from QM/MM free energy simulations for (b) O-O bond breaking step and (c) the β-H abstraction step from the substrate, lauric acid in UndB.

Substrate-triggered activation of O_2 and formation of a peroxodiferric intermediate

Considering the above inactive conformation of UndB and the complexity of its active site, we employed a specialized variant of QM/MM molecular dynamics simulations to gain mechanistic insight into the hydrogen atom abstraction (HAA) process. The simulations used a hybrid QM/MM interface. This method efficiently explores the reaction pathway of UndB in the absence of any prior knowledge of the active state (22). The multiscale simulations were followed by 100ps of unbiased QM/MM MD run. The QM region consists of 312 atoms that involves the diiron center (Fe^{2+}), active site histidines (Asp 88, Glu142, Glu 143, (His89, His93, His128, His131, His132, His261, His297, His300, and His301) (7), the lauric acid substrate, and water molecules within 2.5 Å of the active site (Fig. S8, SI). The unbiased QM/MM MD showed successful abstraction of β-hydrogen by the activated oxygen species and release of carbon dioxide within 15 ps, and the resulting conformation was found to be stable throughout 100 ps. The QM/MM MD simulations were performed with spin state S = 4 and other spin states that best represent electronic state in UndB active site (23). The target of the QM/MM MD simulations is to capture all possible intermediate states of the ESO_2 complex and cross-validate it against experimental results. Moreover, we constructed a cluster model of UndB from the QM/MM MD snapshot which consists of 158 atoms ((Fig. S9, SI) that includes two iron atoms, nine coordinating histidine residues and a lauric acid substrate for investigation using a rigorous quantum chemical method.

To our surprise, QM/MM MD simulations generated one reactive conformation of UndB: a peroxide bridging species, similar to the famous 'P' intermediate reported for sMMO, not its successor 'Q' (12). It also shows product (1-alkene) formation along with release of carbon dioxide (CO_2) in 15 ps. After that, the enzyme-product complex remains stable till 100 ps. Formation of the diferricperoxo intermediate is supported by *ab initio* quantum chemical density functional theory (DFT) calculations. All other O_2 binding to either of the Fe centres converge eventually to the peroxodiferric ESO_2 complex. As stated earlier, QM/MM MD simulations reveal O_2 binds preferably to the Fe_B ion coordinated with the substrate, LA, as is also supported by quantum chemical DFT calculations with anti-ferromagnetically coupled Fe cofactors. Without the LA binding, O_2 does not bind to either of the Fe centres and is not activated for chemical reaction as revealed by longer Fe–O = 2.30 Å (Table S1, SI). It nonetheless implies that this a clear case of substrate-triggered O_2 activation in UndB, as observed in UndA (6), ADO (24) and in other enzymes (12). The Fe_B centre bound to the substrate transfers the first electron to the molecular O_2 for its activation supporting substrate-triggered activation mechanism (Table S2, SI). It may further be noted that a superoxide ESO_2 complex with O_2 bound to the Fe_A centre is only observed in the ferromagnetic state, albeit with O_2 less activated than the peroxide intermediate (O–O = 1.25Å, Table S2, SI). Abstraction of a hydrogen atom from a strong C-H bond of lauric acid (BDE > 95 kcal/mol) by a metal superoxo species appears less likely (6, 25, 26), which is supported by quantum chemical calculations discussed in SI. To get a deeper understanding of the HAA process, we formed QM/MM WT-metadynamics of the major catalytic steps using suitable collective variables.

However, formation of a peroxodiferric intermediate is a very striking observation for an enzyme UndB with longer Fe…Fe distance and also in the absence of any bridging carboxylate ligand or oxo-bridge. Shorter Fe…Fe distance (3.0 - 4.2Å) along with one or more bridging ligands, as observed in sMMO, RNR and in other FDOs, have been a structural hallmark for diferricperoxo intermediate formation (12, 13). The Fe_A-O_A and Fe_B-O_B bond distances in UndB is 1.83Å and 2.12Å (Fig. 3, 1.958 and 1.977Å at the B3LYP-D3/def2-SVP level) respectively. These distances are relatively longer than experimentally observed Fe–O bond lengths (< 1.88 Å)

in diferricperoxo intermediate (12). It points towards a weakly bound or quasi-stable peroxodiferric complex, which can easily leak out in the solution media to produce hydrogen peroxide (H_2O_2). This is strongly supported by *in situ* production of large amounts of H_2O_2 that inhibits UndB catalysis (1). Detection of H_2O_2 has been an important indicator for peroxide intermediate formation as was checked in other $NHFe_2$ enzyme (27). Characterization of such peroxo species in SznF, HmrI and Δ9-Desaturase endowed with longer Fe…Fe distance (> 4.0Å) lends strong credence to it. This kind of peroxo intermediate without any oxo-bridge is reported for heme-oxygenase-like diiron oxidase and oxygenases (HDO) metalloenzyme SznF (28, 29). Thus, for the first time our study unravels the origin of large amount of H_2O_2 production during UndB catalysis and thereby suggest pathways to mitigate it for effective catalysis.

Existence of structurally dynamic iron cofactors in UndB

QM/MM MD simulations indicated that the peroxodiferric intermediate itself is unable to abstract a β-hydrogen from lauric acid. Incidentally the peroxo bond is elongated with assistance from a water molecule (possibly a proton donor) that results in the O–O bond breaking to form a high-valent iron(Fe(IV))-oxo(O) species. It is this iron-oxo species generated from a hydroperoxo intermediate containing an extra electron and proton that abstract a β-hydrogen from the substrate, LA. The diiron-oxo-hydroxo species without a oxo-bridge is similar in nature to the open-core structure of the famous 'Q' intermediate (30). We then performed a QM/MM free energy simulation using well-tempered metadynamics to determine the free energy of activation of the major catalytic steps from this intermediate in UndB in ferromagnetic situation (with S = 4.5). Using two suitable collective variables, the O–O bond breaking step shows a free energy barrier of 10.7 kcal/mol (Fig. 3a,b). Interestingly the free energy barrier of activation for the β-H abstraction by the iron-oxo species is found to be 14.1 kcal/mol, which is calculated to be 15.2 kcal/mol from QM calculations. This is in good agreement with the experimentally obtained barrier of 17.9 kcal/mol (from experimental k_{cat}) considering the usage of a semi-empirical method (23). Our QM/MM free energy calculations also show the β-H abstraction step as the rate determining step (rds) in excellent accord with experimental kinetic isotope effect. Essentiality of extra electrons and proton for UndB catalysis is supported by consumption of four reducing equivalents (NADPH). More support is drawn from a recent study of Arylamine Oxygenases and related binuclear $NHFe_2$ as well as soluble Δ9-Desaturase enzymes where supply of electrons and protons was shown to be indispensable for its catalysis (31, 32). All these results are further validated by cluster model QM calculations. Major catalytic steps involve formation of a (hydro)peroxo intermediate that generate the active iron-oxo species which then perform the rate determining β-H abstraction followed by decarboxylation to generate the product.

We observed an interesting feature in the Fe..Fe distance. During the breaking of the (hydro)peroxo O–O bond, the Fe…Fe distances samples a relatively wide range (4.6Å-6.6Å) of distances (Fig. 4a) It reveals the dynamic nature of two iron cofactors in UndB capable of contracting the Fe-Fe distance in the presence of O_2 and substrate. Attempt to decrease the iron-iron distance without the substrate and co-substrate below 5.0 Å leads to a barrier of 13.0 kcal/mol and above, a result also supported by a combined computational and experimental study on AlkB (14). Existence of such dynamic iron cofactors draws support from different iron-iron distance reported for multiple resolved structures of AlkB and SCD1. Generally shorter interatomic

distance between the iron centers is essential for formation of the peroxodiferric intermediate as has been well-documented in several studies (12).

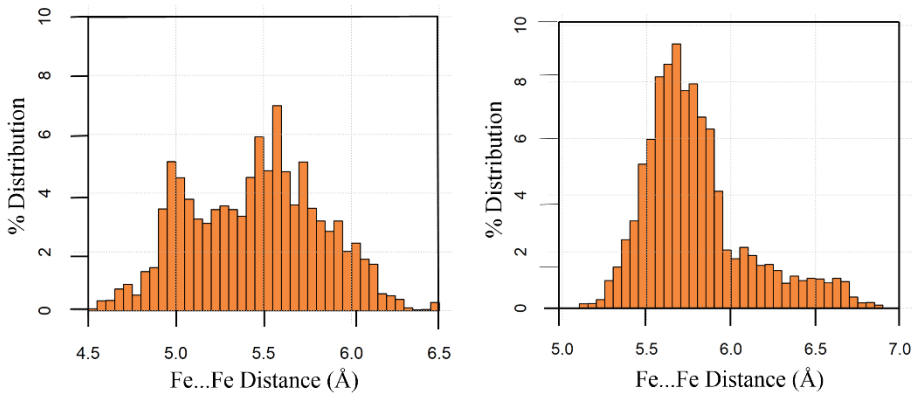

Fig. 4. Histogram population analysis of Fe…Fe distances during (left) (hydro)peroxo-to-oxo intermediate formation and (right) the β-H abstraction step from QM/MM metadynamics simulation of PcUndB.

This anti-ferromagnetic coupling of the two iron centers through a dioxygen-derived peroxo bridge that most possibly explain the coupled diiron cofactors with an anti-ferromagnetic (AF) coupling constant of $J \approx 15\ cm^{-1}$. The coupling constant values matches well with those values for dioxygen-derived bridges as reported by Solomon and coworkers (32). The quasi-stable nature or fleeting existence of the peroxodiiron(III/III) species is probably responsible for its escape detection by any method.

Conclusions

Our study has deciphered the enigmatic molecular mechanism of conversion of free fatty acids to terminal alkenes by UndB using O_2 using a multiscale dynamical approach. The most important outcome is discovering the existence of dynamic iron cofactors in UndB endowed with characteristic longer iron-iron separation. The flexible iron centers is capable of forming a quasi-stable μ-1,2-peroxodirron(III/III) intermediate to activate molecular O_2 to produce 1-alkene. UndB has emerged a rare example where this dynamic iron coordination sites gets clearly manifested in large production of H_2O_2 through formation of a peroxodirron(III/III) species despite large separation between iron centers along with absence of any bridging residues. This mechanism accounts for all major experimental findings and in good agreement with the observed activation barrier. The comprehensive mechanism presented in this paper would enrich the growing understanding of various elegant strategies nature employs to use O_2 to perform difficult biochemical reactions. This work may thus open a new window to understand how such metalloenzymes work in unprecedented details.

Methods

Considering the remarkable success in predicting correct 3D structures of proteins from its amino acid sequences, we have used Alphafold3 to generate an initial structure of UndB from its amino acid sequences. The initial structure for model preparation was generated using AlphaFold3 (10) using the (UniProt ID: A4Y0K1) and (GenBank: UKZ44198.1), with Fe ions incorporated into the

active site through the AlphaFold3 method. From the sequences generated by AlphaFold3, the structure with the highest confidence was selected for system preparation. A total of 2.1 μs of all-atom simulations were performed using a timestep of 1 fs. Trajectory analysis was performed using the VMD(33) program. Molecular dynamics (MD) simulations were performed using the GPU-accelerated version of the NAMD(34) package. The PM6 (35) method was employed for the QM region using the NAMD-MOPAC interface (36), while the MM subsystem was treated with CHARMM36 force field (37). We created the cluster models(43) for quantum chemical calculations from appropriate snapshots of QM/MM MD simulations trajectory. All quantum chemical (QM) calculations were carried out with the density functional theory (DFT) method as implemented in the ORCA program package.(37) The QM region for all the QM/MM MD simulations consists of the diiron center (Fe^{2+}), active site histidines (His89, His93, His128, His131, His132, His261, His297, His300, and His301) (7), the lauric acid substrate, and water molecules within 2.5Å of the active site. The VMD-QwikMD interface was used for system set up (38). The equilibrated intermediate structure was used as an initial structure for QM/MM well-tempered metadynamics (WT-MetaD) (39, 40) simulations to enhance sampling along the collective variable space. All other simulation parameters were identical to those used in classical molecular dynamics.

ASSOCIATED CONTENT

Supporting Information. Computational methods, molecular dynamics data and Cartesian coordinates of calculated structures.

AUTHOR INFORMATION

Corresponding Author

Subhendu Roy - *Biophysical Sciences Group, Saha Institute of Nuclear Physics, Kolkata 700064, India. Homi Bhabha National Institute, Mumbai 400094, India.*

Authors

Simran Nisha and Arunima Choudhury have equally contributed to this paper.

Simran Nisha - *Crystallography & Molecular Biology Division, Saha Institute of Nuclear Physics, Kolkata 700064, India.*

Arunima Choudhury - *Crystallography & Molecular Biology Division, Saha Institute of Nuclear Physics, Kolkata 700064, India.*

ACKNOWLEDGMENT

S. R. acknowledges support from Ramalingaswami Re-entry Fellowship (BT/RLF/Re-entry/39/2017), Department of Biotechnology, India. S. N. acknowledges doctoral fellowship from DBT, Govt. of India and A.C. thanks SINP for her doctoral fellowship. The financial support from

DAE-Saha Institute of Nuclear Physics, Kolkata is duly acknowledged. We thank SINP computing facility for the computational resources.

Data Availability

All data are available in the main text and SI Appendix.

Competing Interest Statement: The authors declare no competing interest.

References

1. T. Iqbal, S. Murugan, D. Das, A chimeric membrane enzyme and an engineered whole-cell biocatalyst for efficient 1-alkene production. *Sci Adv* **10**, eadl2492 (2024).
2. T. Iqbal, S. Chakraborty, S. Murugan, D. Das, Metalloenzymes for Fatty Acid-Derived Hydrocarbon Biosynthesis: Nature's Cryptic Catalysts. *Chem Asian J* **17**, e202200105 (2022).
3. T. Iqbal, S. Murugan, K. Rajendran, J. S. Sidhu, D. Das, Unraveling the Conversion of Fatty Acids into Terminal Alkenes by an Integral Membrane Enzyme, UndB. *ACS Catalysis* **13**, 15516-15525 (2023).
4. J. Shen, G. Wu, A.-L. Tsai, M. Zhou, Structure and Mechanism of a Unique Diiron Center in Mammalian Stearoyl-CoA Desaturase. *Journal of Molecular Biology* **432**, 5152-5161 (2020).
5. X. Guo *et al.*, Structure and mechanism of the alkane-oxidizing enzyme AlkB. *Nat Commun* **14**, 2180 (2023).
6. B. Zhang *et al.*, Substrate-Triggered Formation of a Peroxo-Fe(2)(III/III) Intermediate during Fatty Acid Decarboxylation by UndA. *J Am Chem Soc* **141**, 14510-14514 (2019).
7. Z. Rui, N. C. Harris, X. Zhu, W. Huang, W. Zhang, Discovery of a Family of Desaturase-Like Enzymes for 1-Alkene Biosynthesis. *ACS Catalysis* **5**, 7091-7094 (2015).
8. A. B. Jacobs *et al.*, Nuclear Resonance Vibrational Spectroscopic Definition of the Fe(IV)(2) Intermediate Q in Methane Monooxygenase and Its Reactivity. *J Am Chem Soc* **143**, 16007-16029 (2021).
9. J. Shen, G. Wu, A. L. Tsai, M. Zhou, Structure and Mechanism of a Unique Diiron Center in Mammalian Stearoyl-CoA Desaturase. *J Mol Biol* **432**, 5152-5161 (2020).
10. Anonymous, Structure of AlkB-AlkG shows details of alkane terminal C-H selectivity and functionalization. *Nat Struct Mol Biol* **30**, 413-414 (2023).
11. J. T. Groves, L. Feng, R. N. Austin, Structure and Function of Alkane Monooxygenase (AlkB). *Acc Chem Res* **56**, 3665-3675 (2023).
12. A. J. Jasniewski, L. Que, Jr., Dioxygen Activation by Nonheme Diiron Enzymes: Diverse Dioxygen Adducts, High-Valent Intermediates, and Related Model Complexes. *Chem Rev* **118**, 2554-2592 (2018).
13. S. R. Pope *et al.*, Heme Oxygenase-Like Metalloenzymes. *Annu Rev Biochem* **94**, 59-88 (2025).

14. C. R. Reinhardt *et al.*, No Bridge between Us: EXAFS and Computations Confirm Two Distant Iron Ions Comprise the Active Site of Alkane Monooxygenase (AlkB). *J Am Chem Soc* **147**, 2432-2443 (2025).
15. M.-J. Yu, S.-L. Chen, From Alkane to Alkene: The Inert Aliphatic C–H Bond Activation Presented by Binuclear Iron Stearoyl-CoA Desaturase with a Long di-Fe Distance of 6 Å. *ACS Catalysis* **9**, 4345-4359 (2019).
16. J. Chai, G. Guo, S. M. McSweeney, J. Shanklin, Q. Liu, Structural basis for enzymatic terminal C-H bond functionalization of alkanes. *Nat Struct Mol Biol* **30**, 521-526 (2023).
17. Anonymous, <Alkb-maussbauer-pnas-1997.pdf>.
18. J. Shen, G. Wu, B. S. Pierce, A. L. Tsai, M. Zhou, Free ferrous ions sustain activity of mammalian stearoyl-CoA desaturase-1. *J Biol Chem* **299**, 104897 (2023).
19. Anonymous, <AlkB-AF-coupled-pnas-1997.pdf>.
20. J. Abramson *et al.*, Accurate structure prediction of biomolecular interactions with AlphaFold 3. *Nature* **630**, 493-500 (2024).
21. A. B. Petroff, R. L. Weir, C. R. Yates, J. D. Ng, J. Baudry, Sequential Dynamics of Stearoyl-CoA Desaturase-1(SCD1)/Ligand Binding and Unbinding Mechanism: A Computational Study. *Biomolecules* **11** (2021).
22. S. Makurat, R. P. P. Neves, M. J. Ramos, J. Rak, QM/MM MD Study on the Reaction Mechanism of Thymidine Phosphorylation Catalyzed by the Enzyme Thermotoga maritima Thymidine Kinase 1. *ACS Catalysis* **14**, 9840-9849 (2024).
23. J. Čivić, I. Tuñón, J. N. Harvey, Understanding Substrate Binding and Reactivity of Stearoyl-CoA Desaturase (SCD1) through Classical and Multiscale Molecular Dynamics Simulations. *ACS Catalysis* **15**, 1684-1692 (2025).
24. T. R. K. Rana *et al.*, Biofuel Production by Aldehyde-Deformylating Oxygenase: Insights into Spin States, Spin Coupling, and Diiron Cofactor Reactivity Using Multiscale Modeling. *Inorg Chem* **65**, 1561-1573 (2026).
25. W. A. van der Donk, C. Krebs, J. M. Bollinger, Jr., Substrate activation by iron superoxo intermediates. *Curr Opin Struct Biol* **20**, 673-683 (2010).
26. J. M. Bollinger, Jr., C. Krebs, Enzymatic C-H activation by metal-superoxo intermediates. *Curr Opin Chem Biol* **11**, 151-158 (2007).
27. O. M. Manley *et al.*, BesC Initiates C-C Cleavage through a Substrate-Triggered and Reactive Diferric-Peroxo Intermediate. *J Am Chem Soc* **143**, 21416-21424 (2021).
28. J. Liu, Z. Wang, X. Sang, X. Zhang, B. Wang, Peroxo-Diiron(III/III) as the Reactive Intermediate for N-Hydroxylation Reactions in the Multidomain Metalloenzyme SznF: Evidence from Molecular Dynamics and Quantum Mechanical/Molecular Mechanical Calculations. *ACS Catalysis* **13**, 5808-5818 (2023).
29. M. J. McBride *et al.*, A Peroxodiiron(III/III) Intermediate Mediating Both N-Hydroxylation Steps in Biosynthesis of the N-Nitrosourea Pharmacophore of Streptozotocin by the Multi-domain Metalloenzyme SznF. *J Am Chem Soc* **142**, 11818-11828 (2020).
30. C. E. Schulz, R. G. Castillo, D. A. Pantazis, S. DeBeer, F. Neese, Structure-Spectroscopy Correlations for Intermediate Q of Soluble Methane Monooxygenase: Insights from QM/MM Calculations. *J Am Chem Soc* **143**, 6560-6577 (2021).
31. D. Bim *et al.*, Proton-Electron Transfer to the Active Site Is Essential for the Reaction Mechanism of Soluble Delta(9)-Desaturase. *J Am Chem Soc* **142**, 10412-10423 (2020).

32. L. H. Bottger *et al.*, Nature of the Reactive Biferric Peroxy Intermediate P' in the Arylamine Oxygenases and Related Binuclear Fe Enzymes. *J Am Chem Soc* **147**, 11707-11725 (2025).
33. W. Humphrey, A. Dalke, K. Schulten, VMD: Visual molecular dynamics. *Journal of Molecular Graphics* **14**, 33-38 (1996).
34. J. C. Phillips *et al.*, Scalable molecular dynamics with NAMD. *Journal of Computational Chemistry* **26**, 1781-1802 (2005).
35. J. J. P. Stewart, A. C. Stewart, A semiempirical method optimized for modeling proteins. *Journal of Molecular Modeling* **29** (2023).
36. M. C. R. Melo *et al.*, NAMD goes quantum: an integrative suite for hybrid simulations. *Nature Methods* **15**, 351-354 (2018).
37. K. Vanommeslaeghe *et al.*, CHARMM general force field: A force field for drug-like molecules compatible with the CHARMM all-atom additive biological force fields. *Journal of Computational Chemistry* **31**, 671-690 (2010).
38. J. V. Ribeiro *et al.*, QwikMD — Integrative Molecular Dynamics Toolkit for Novices and Experts. *Scientific Reports* **6**, 26536 (2016).
39. V. D. Trivedi *et al.*, In-depth Sequence-Function Characterization Reveals Multiple Pathways to Enhance Enzymatic Activity. *ACS Catal* **12**, 2381-2396 (2022).
40. A. Barducci, G. Bussi, M. Parrinello, Well-Tempered Metadynamics: A Smoothly Converging and Tunable Free-Energy Method. *Physical Review Letters* **100** (2008).